AFRL-AFOSR-UK-TR-2017-0013

Nonlinear light dynamics in multi-core structures

Sergei Turitsyn
ASTON UNIVERSITY

02/27/2017
Final Report

Air Force Research Laboratory
AF Office Of Scientific Research (AFOSR)/ IOE
Arlington, Virginia 22203
Air Force Materiel Command

REPORT DOCUMENTATION PAGE

Form Approved
OMB No. 0704-0188

1. REPORT DATE *(DD-MM-YYYY)*	2. REPORT TYPE	3. DATES COVERED *(From - To)*
27-02-2017	Final	30 Sep 2014 to 29 Sep 2016

4. TITLE AND SUBTITLE
Nonlinear light dynamics in multi-core structures

5a. CONTRACT NUMBER

5b. GRANT NUMBER
FA9550-14-1-0305

5c. PROGRAM ELEMENT NUMBER
61102F

6. AUTHOR(S)
Sergei Turitsyn

5d. PROJECT NUMBER

5e. TASK NUMBER

5f. WORK UNIT NUMBER

7. PERFORMING ORGANIZATION NAME(S) AND ADDRESS(ES)
ASTON UNIVERSITY
ASTON TRIANGLE
BIRMINGHAM, B4 7ET GB

8. PERFORMING ORGANIZATION REPORT NUMBER

9. SPONSORING/MONITORING AGENCY NAME(S) AND ADDRESS(ES)
EOARD
Unit 4515
APO AE 09421-4515

10. SPONSOR/MONITOR'S ACRONYM(S)
AFRL/AFOSR IOE

11. SPONSOR/MONITOR'S REPORT NUMBER(S)
AFRL-AFOSR-UK-TR-2017-0013

12. DISTRIBUTION/AVAILABILITY STATEMENT
A DISTRIBUTION UNLIMITED: PB Public Release

13. SUPPLEMENTARY NOTES

14. ABSTRACT
The project has led to a number of results, including introduction of the key mathematical models governing optical field propagation in the multiple-core structures (e.g. waveguides and fibers); study of the properties of light-bullets fully localized both in space and time that can be generated in continuous-discrete optical media such as multi-core optical fiber or waveguide arrays; localisation dynamics in a continuous-discrete nonlinear system. Detailed theoretical analysis is presented of the existence and stability of the discrete-continuous light bullets using a very generic model that occurs in a number of application, study of the steady state propagation
regimes, study of the modulation instability in multiple-core fibers (MCFs), investigation of the nonlinear stage of the instability and energy transfer. A numerical demonstration of a light pulse combining and pulse compression using wave collapse (self-focusing) energy localisation dynamics in a continuous-discrete nonlinear system, as implemented in a MCF using 1D and 2D core distribution designs. Large-scale numerical simulations were performed to determine the conditions of the most efficient coherent combining and compression of pulses injected into the considered MCFs.

15. SUBJECT TERMS
fibre lasers, coherent beam combining, discrete vortices orbital angular momentum, Nonlinear light dynamics, EOARD

16. SECURITY CLASSIFICATION OF:			17. LIMITATION OF ABSTRACT	18. NUMBER OF PAGES	19a. NAME OF RESPONSIBLE PERSON
a. REPORT	b. ABSTRACT	c. THIS PAGE			CUMMINGS, RUSSELL
Unclassified	Unclassified	Unclassified	SAR	27	19b. TELEPHONE NUMBER *(Include area code)* 011-44-1895-616021

Standard Form 298 (Rev. 8/98)
Prescribed by ANSI Std. Z39.18

EUROPEAN OFFICE OF AEROSPACE RESEARCH AND DEVELOPMENT

Final Report

PI: Prof. Sergei K. Turitsyn

Institution: *Aston Institute of Photonic Technologies, Aston University*

AFOSR award number: FA9550-14-1-0305

Nonlinear light dynamics in multi-core structures

Summary. This report presents the results of the research activities within the project FA9550-14-1-0305. The project has led to a number of results, including introduction of the key mathematical models governing optical field propagation in the multiple-core structures (e.g. waveguides and fibers); study of the properties of light-bullets fully localized both in space and time that can be generated in continuous-discrete optical media such as multi-core optical fiber or waveguide arrays; localisation dynamics in a continuous-discrete nonlinear system. We present detailed theoretical analysis of the existence and stability of the discrete-continuous light bullets using a very generic model that occurs in a number of application, study of the steady state propagation regimes, study of the modulation instability in multiple-core fibers (MCFs), investigation of the nonlinear stage of the instability and energy transfer. We demonstrated numerically light pulse combining and pulse compression using wave collapse (self-focusing) energy localisation dynamics in a continuous-discrete nonlinear system, as implemented in a MCF using 1D and 2D core distribution designs. Large-scale numerical simulations were performed to determine the conditions of the most efficient coherent combining and compression of pulses injected into the considered MCFs. We demonstrated the possibility of combining in a single core 90% of the total

energy of pulses initially injected into all cores of a 7-core MCF with a hexagonal lattice. A pulse compression factor of about 720 can be obtained with a 19-core ring MCF.

1. Introduction

Fast growing powers of modern optical devices make underlying dynamics and evolution of fields and beams essentially nonlinear. An important example is high-power fiber lasers. The fiber laser manufacturing has been greatly enhanced by the technologies developed in the telecom industry, but the recently emerged applications (and markets) include so different areas as medicine, metrology, defence, spectroscopy, industrial cutting, welding, with the list of new applications growing very fast. Fiber lasers hold a number of attractions including compactness, very good cooling characteristics and high quality of emitted light. Fiber lasers are widely considered now as promising technology of producing efficient high-power coherent light sources. However, fiber laser's brightness is limited by the variety of nonlinear effects. As the power level of fiber sources increases, nonlinear effects become increasingly important. Understanding and controlling nonlinear effects in multi-core fiber holds the key to unlocking new techniques and technologies. A number of engineering and physical techniques are used to scale laser power up.

Mathematical modelling plays a crucial role in building platform for new progress in this field. Nonlinear dynamics in discrete systems is an interdisciplinary research field that has links to a large number of areas of science and technology. This is both because matter itself is described by discrete models and also because many important engineering nonlinear systems are based on few interacting constituents or elements. Nonlinear discrete systems describe a variety of phenomena in condensed matter, nonlinear optics, biology and other fields; from energy transport in molecular chains and protein molecules to light propagation in waveguide arrays. A number of different physical systems can be effectively described by the same mathematical models. In this report we present generic and practically very important example of low-dimension nonlinear discrete systems – light propagation in multi-core fiber and demonstrate new features introduced by discrete multi-core propagation.

Structuring of light in space and time is a fascinating area of research and technology. In space, light can be localized and structured by using wave-guides that are formed by appropriate variations of the refractive index. Nonlinear optics gives another practical possibility to localize and control light both in space and time. The combination of these two features leads to a rich variety of interconnected methods to structure and manipulate spatial and temporal properties of light. In particular, advances in fiber optics technology over the past 30 years, has had an impact not only in numerous highly important applications, but it has also provided a laboratory to display nonlinear phenomena such as modulation instability, solitons formation and interactions, super-continuum generation, parametric amplification, optical wave turbulence and many others. In space, even earlier, the possibility of balancing diffraction with nonlinear self-focusing so that localized wave-packets could propagate undistorted emerged as an important topic with broad applicability.

At that time, the theory of soliton formation and its instability in the 1+2 dimensional nonlinear Schrödinger equation (NLSE), $i\partial_z u(x,y;z)+\Delta_T u+|u|^{2\sigma}u=0$, proved that for the Kerr nonlinearity (σ=1), a 2-d spatial soliton is unstable in that it either collapses (for powers above critical) or diffracts. In this equation, *u* represents the envelope of the electric field; (*x,y)* are the spatial variables transverse to the direction of propagation *z.* At this so called critical (σd=2, d=transverse dimension), critical collapse is easily arrested by many additional terms in the model even if small. Most common examples are losses, nonlinear saturation. In particular if instead of a continuum field we have a discrete model with the corresponding discrete Laplacian, in the earlier seminal work [1,2] demonstrated in a particular rectangular geometry of waveguide arrays that stable bullets propagate in such model. Recent technological advances in photonic crystals and multi-core fibers made possible new demonstrations of light localization. While multi-core fiber technology was driven by major challenges in optical communication in providing methods and techniques capable to offer transmission capacity above the limitations of the single mode-fiber communication channels [3,4]. A multi-core fiber (MCF) allows one to implement spatial division multiplexing, enabling a scale-up in transmission capacity per-fiber and more recently, they were used for the experimental demonstration of Light Bullets (LB) in a multi-core optical array [5,6]. Furthermore, as the technology of multicore fibers continues to advance so are the possible applications of such arrays. Spatial de-multiplexing is also important in emerging applications of multi-core fiber is in the field of high-power fiber lasers [7,8]. The reason this technology has been instrumental in novel design of fiber lasers is the limitation in generating high power outputs in a single laser. The power transmitted through the single mode fiber is limited by the different non-linear effects. To overcome this threshold and generate high powers, a promising approach is to coherently combine multiple amplifier outputs. Here, the use of multi-core fiber allows one to split the total high power into channels with power below any undesirable nonlinear effects. In other words, laser beams in each core may be transported safely being below the threshold of the detrimental nonlinear effects while the total coherently combined power can be high. In recent work [8] multi-core fibers in a hexagonal configuration was used to efficiently combine the output of multiple fiber amplifiers so that one can produce coherent output power that scales to the number of cores (equal to the number of amplifiers). We should emphasize that a critical component of the coherent beam combining scheme, is the ability to design of multicore structures with a geometrical configuration that has a more general coupling scheme that the simplest nearest neighbor. In this respect, our work presented here represents an important contribution to this application in that it studies for the first time the stability properties of LB under more general coupling schemes. Finally, this new multi-core fiber technology opens up new perspectives for the fascinating research on light bullets (see e.g. [9-15] and references therein) and can be a natural laboratory to study fundamental phenomena such as nonlinear Anderson localization, light filaments and vortices and optical rogue wave formation to name some. The MCF is a specific realization of fiber arrays with flexible mutual arrangement of cores. It is important to understand how the mutual arrangement of fibers will affect the existence the LB and their stability, which is the subject of present paper

Given the importance of LB in nonlinear science and applications mentioned above, the main objective of this work was to analyze the optical bullet features in continuous-discrete optical media including their stability under the most general coupling schemes. Our focus is on the generic models that may be applied in various applications. This theoretical work we believe will provide a

framework in the design of multicore elements aiming at optimizing desirable and specific applications such as routing, switching and coherent beam combining.

2. MATHEMATICAL DESCRIPTION OF THE SYSTEM

For arrays of waveguides where light propagates mainly in the central (core) region of the individual elements and for which transverse exchange of energy is due to tails of the field overlapping neighbor waveguides, the field is well approximated by a superposition $E(x,y,z,t)=\sum_{nm}U_{nm}(z,t)F(x-x_n,y-y_m)e^{i(kz-\omega t)}+cc$ where we assume each waveguide is identical and supports a single mode *F*. The center of each waveguide is at location (x_n,y_m).

2.1 Basic equations

The equations, in dimensionless form, describing the propagation of the envelopes $U_{nm}(z,t)$ propagating in the fiber at site (*n,m)* read:

$$i\partial_z U_{nm}+(\underline{\underline{C}}\underline{U})_{nm}+\partial_{t^2}^2 U_{nm}+2|U_{nm}|^2 U_{nm}=0 \qquad (1)$$

where $(\underline{\underline{C}}\underline{U})_{nm}$ represents the linear coupling profile at site (*n,m*). Two cases of interest are the uniform square and hexagonal geometries, for which the respective coupling operators are (see Figure 1)

$$(\underline{\underline{C}}\underline{U})_{nm}^{square}=c(U_{n-1,m}+U_{n+1,m}+U_{n,m-1}+U_{n,m+1}) \qquad (2a)$$

$$(\underline{\underline{C}}\underline{U})_{nm}^{hexagon}=c(U_{n-1,m-1}+U_{n-1,m+1}+U_{n,m-2}+U_{n,m+2}+U_{n+1,m-1}+U_{n+1,m+1}) \qquad (2b)$$

This system has two known conserved quantities; the Hamiltonian $H=\sum_{nm}\int(N(\underline{U};\underline{U})_{nm}+|\partial_t U_{nm}|^2-|U_{nm}|^4)dt$ and the total power $P=\sum_{nm}\int|U_{nm}|^2\,dt$.

The form of the discrete-continuous light bullets (that are extrema of the Hamiltonian under fixed total power P) $U_{nm}(z,t)=A_{nm}(t,\lambda)e^{i\lambda z}$ is given by the equation:

$$-\frac{\delta}{\delta U_{nm}^*}(H+\lambda P)=-\lambda U_{nm}+(\underline{\underline{C}}\underline{U})_{nm}+\partial_{t^2}^2 U_{nm}+2|U_{nm}|^2 U_{nm}=0 \qquad (3)$$

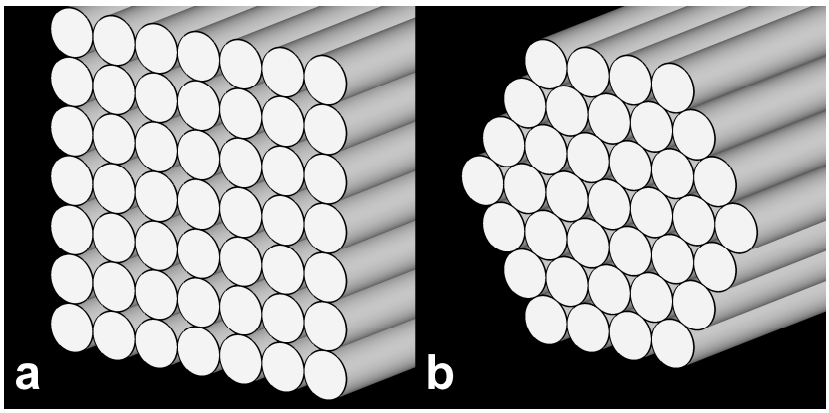

Figure 1. Square and hexagonal waveguides structures

2.2 Localized bullet solutions

Highly localized bullet solutions in some limits can be derived using an asymptotic approach. The consideration is that spatially most of the energy is concentrated in one site, (0,0) and small satellite pulses of decreasing amplitude propagate in subsequent layers. Mathematically, this means we seek solutions of the form $U_{nm}(z,t) = A_{nm}(t)e^{i\lambda z}$ with $\lambda >> 1$, where each envelope has an expansion of the form $A_{nm}(t) = A_{nm}^{(0)}(t;\lambda) + A_{nm}^{(1)}(t;\lambda) + A_{nm}^{(2)}(t;\lambda) + ...$

We only present the solutions for the central core and first layer: The functional form is the same for the central core, the second line gives the functional form for the first layer in the square array, while the third gives the form for the first layer of hexagonal array

$$A_{00}(t) = a_0(t) + O(\frac{1}{\lambda^{3/2}}) = \frac{\sqrt{\lambda}}{\cosh(\sqrt{\lambda}\, t)} + O(\frac{1}{\lambda^{3/2}})$$

$$A_{\pm1,0}(t) = A_{0,\pm1} = a_1(t) + O(\frac{1}{\lambda^{5/2}}) = \frac{c}{2\sqrt{\lambda}}[e^{\sqrt{\lambda}t}\ln(1+e^{-2\sqrt{\lambda}t}) + e^{-\sqrt{\lambda}t}\ln(1+e^{2\sqrt{\lambda}t})] + O(\frac{1}{\lambda^{5/2}})$$

$$A_{0,\pm2}(t) = A_{1,\pm1}(t) = A_{-1,\pm1}(t) = a_1(t) + O(\frac{1}{\lambda^{3/2}}) = \frac{c}{2\sqrt{\lambda}}[e^{\sqrt{\lambda}t}\ln(1+e^{-2\sqrt{\lambda}t}) + e^{-\sqrt{\lambda}t}\ln(1+e^{2\sqrt{\lambda}t})] + O(\frac{1}{\lambda^{3/2}})$$

(4)

These solutions fail to be uniformly valid beyond $|t \geq O(\lambda)$. In fact at the pulse tails, all waveguides have solutions of the same order $A_{nm} = O(\lambda e^{-\lambda|t|}), t \geq \lambda$.

What follows are numerical simulations corresponding to these highly localized solutions as well as more general nonlinear states.

2.3 Numerical simulations

We calculate now numerically exact solutions describing continuous discrete light bullets in the equation (1) where we varied the number of elements in the array, which is an important consideration for practical systems where the number of cores is finite. The asymptotic functions $a_0(t), a_1(t)$ coincide with numerical solutions $A_{00}(t)$ and $A_{\pm1,0}(t) = A_{0,\pm1}(t)$ of the system (3) up to the order $O(\frac{1}{\sqrt{\lambda}^3})$.

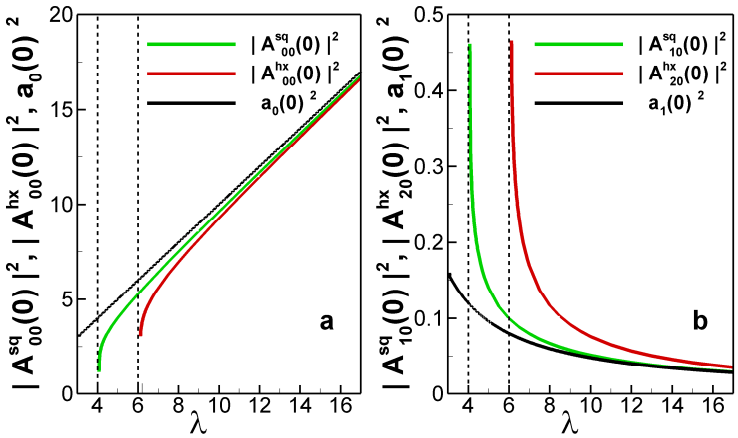

Figure 2 Dependence numerical (color) and theory (black) peak powers vs the parameter λ in central (a) and closer neighbor waveguides (b) for 33x33 square and 65x33 hexagonal waveguides structures

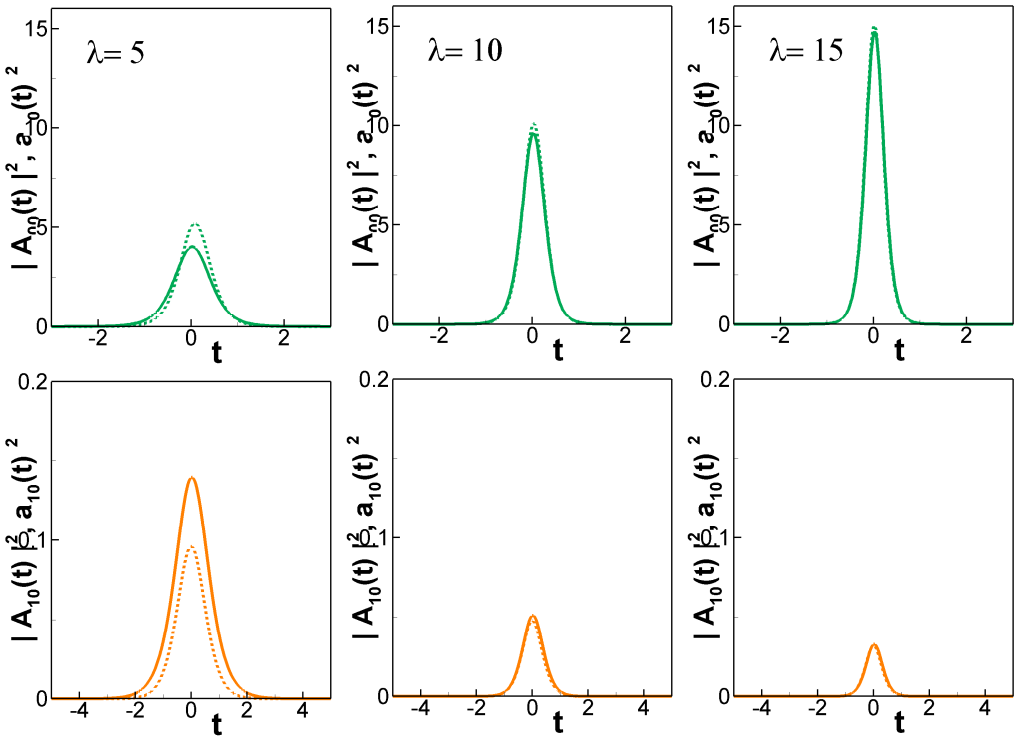

Figure 3 Comparison of numerical solutions (solid) with their analytical approximations (dashed) for different λ in the central waveguide (top green) and closer neighbor waveguide (bottom)

To fully assess the validity of the asymptotic analysis, we compared them with full numerical solutions for the case of a coupling constant c=1 and for the rectangular structure with NxN crossed. Figure 2 shows dependence numerical (color) and theory (black) peak powers versus the parameter λ in central (a) and closer neighbor waveguides (b) for 33x33 square and 65x33 hexagonal waveguides structures. As Figures 2 and 3 show, there is good correspondence between the theory and numerical modeling for large values of λ. Figure 3 shows comparison of the time domain structure of the light bullets for three different values of λ. As expected correspondence is good for value of λ equal to 14 and fails at λ= 7, thus the limiting value of λ for which the asymptotic state is valid is around $\lambda_c \approx 4$. Finally, global quantities of the LB such as power and the Hamiltonian are shown in Figure 4. Here we observed universal behavior for different number of fiber elements. Specific to the power dependence on λ, below we discuss how it relates to the stability properties of the LB.

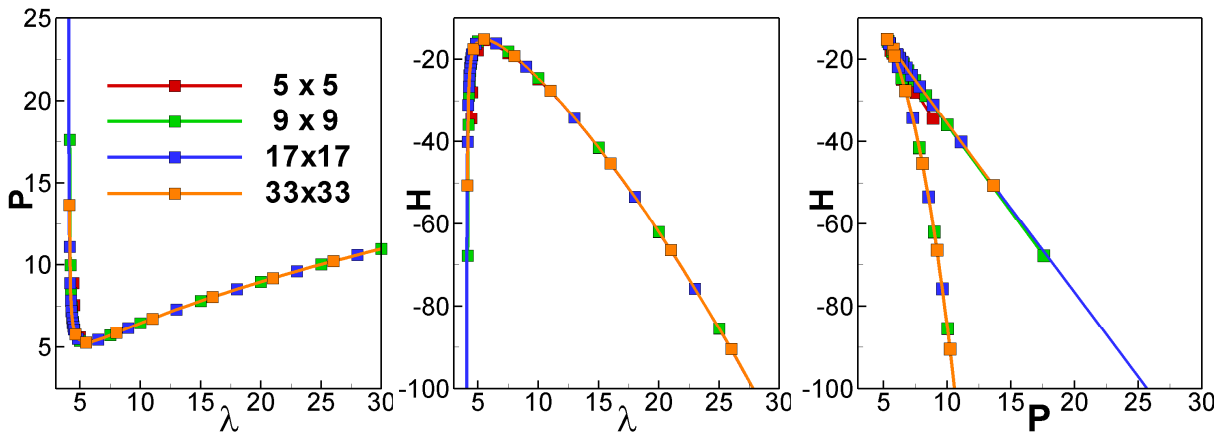

Figure 4 From left to right: dependence of the total power on the parameter λ; dependence of the Hamiltonian on the parameter λ; the Hamiltonian vs the total power

2.4 Stability analysis

We now investigate the stability of solutions of the form $U_{nm}(z,t) = A_{nm}(t)e^{i\lambda z}$ by linearization $U_{nm}(z,t) = (A_{nm}(t) + f_{nm} + ig_{nm})e^{i\lambda z}$, leading to the system of linear equations

$$-\partial_z g_{nm} = -(\underline{\underline{C}}\,\underline{f})_{nm} - \partial_{t^2}^2 f_{nm} + \lambda f_{nm} - 6|A_{nm}|^2 f_{nm} = (H_- f)_{nm}$$

$$\partial_z f_{nm} = -(\underline{\underline{C}}\,\underline{g})_{nm} - \partial_{t^2}^2 g_{nm} + \lambda g_{nm} - 2|A_{nm}|^2 g_{nm} = (H_+ g)_{nm}$$

or

$$-\partial_{z^2}^2 f_{nm} = [H_+(H_- f)]_{nm}$$

For square arrays

$$\langle \underline{f}, H_+ \underline{f} \rangle \equiv \sum_{nm} \int f_{nm}(H_+ f)_{nm}\, dt = \sum_{nm} \int \left[A_{nm}^2 \left(\partial_t \left(\frac{f_{nm}}{A_{nm}} \right) \right)^2 dt \right] + \sum_{nm} \int \left[\left(\sqrt{\frac{A_{n,m-1}}{A_{nm}}} f_{nm} - \sqrt{\frac{A_{n,m}}{A_{n,m-1}}} f_{n,m-1} \right)^2 dt \right]$$

$$+ \sum_{nm} \int \left[\left(\sqrt{\frac{A_{n-1,m}}{A_{nm}}} f_{nm} - \sqrt{\frac{A_{n,m}}{A_{n-1,m}}} f_{n-1,m} \right)^2 dt \right]$$

and for hexagonal arrays

`

$$\langle \underline{f}, H_+ \underline{f} \rangle \equiv \sum_{nm} \int f_{nm}(H_+ f)_{nm}\, dt = \sum_{nm} \int \left[A_{nm}^2 \left(\partial_t \left(\frac{f_{nm}}{A_{nm}} \right) \right)^2 dt \right] + \sum_{nm} \int \left[\left(\sqrt{\frac{A_{n,m-1}}{A_{nm}}} f_{nm} - \sqrt{\frac{A_{n,m}}{A_{n,m-1}}} f_{n,m-1} \right)^2 dt \right]$$

$$+ \sum_{nm} \int \left[\left(\sqrt{\frac{A_{n-1,m}}{A_{nm}}} f_{nm} - \sqrt{\frac{A_{n,m}}{A_{n-1,m}}} f_{n-1,m} \right)^2 dt \right] + \sum_{nm} \int \left[\left(\sqrt{\frac{A_{n+1,m+1}}{A_{nm}}} f_{nm} - \sqrt{\frac{A_{n,m}}{A_{n+1,m+1}}} f_{n+1,m+1} \right)^2 dt \right]$$

$$+ \sum_{nm} \int \left[\left(\sqrt{\frac{A_{n+1,m-1}}{A_{nm}}} f_{nm} - \sqrt{\frac{A_{n,m}}{A_{n+1,m-1}}} f_{n+1,m-1} \right)^2 dt \right]$$

In both cases and similar to the 1+1+1 case [16,17,18] the following properties of the linear operators

hold:

(i) $\langle \underline{f}, H_+ \underline{f} \rangle \geq 0$ and it is equal to 0 if $f_{nm} = 0$ or $f_{nm} = A_{nm}$.

(ii) There exist some $\underline{F}$ for which $\langle \underline{F}, H_- \underline{F} \rangle < 0, \langle \underline{F}, \underline{A} \rangle = 0$

While we present two specific geometries, (i) and (ii) will be generally true for a large class of coupling schemes.

Properties (i) and (ii) allows us to conclude that the existence of negative eigenvalues of the operator H_- is a sufficient condition for instability of the nonlinear state $\underline{A}$. Furthermore one can show this condition is equivalent to the Vakhitov-Kolokolov condition on the sign of $\frac{d}{d\lambda} P = \frac{d}{d\lambda} \langle \underline{A}, \underline{A} \rangle$.

For the highly localized solutions of the previous section, one finds that the power $P(\lambda) = 2\lambda + \frac{K}{\lambda^3}$, where the constant *K* depends on the coupling coefficient and the geometry. Observe that a minimum is achieved at $\lambda_c = \left(\frac{3K}{2} \right)^{1/4}$, so that stability of the localized (λ>1) bullet is assured for

coupling strengths below some critical value $K_c = 2/3$. This stability criterion is also in agreement with the known stability of one dimensional solitons which in this model corresponds to the limit $K \to 0$. As it was the case above, this result is consistent to that shown in figure 2c in [4].

So far, we have demonstrated the existence and stability of the LB localized in several fibers. Now we will demonstrate that the LB can be formed during the propagation of an initial pulse lunched from the input faces of the array. Specifically, we simulate the propagation of a Gaussian pulse lunched in one fiber for the hexagonal geometry. Figure 5 summarizes the general picture: The left panel highlights the propagation for smaller input peak power and broader pulse, where according to our analysis, stable LB do not exist. One can observe fast diffraction (in space) and dispersion (in time) of the pulse. The energy in the central core vanishes after z = 2 being spread through the surrounding layers. For slightly higher peak power (right panel) we observe the formation of LB localized in central fiber and the surrounding layer. The temporal oscillation can be explained in the following way. The Hamiltonian is conserved in our system and in general the initial value of H and that of the LB are different. The adjustment of Hamiltonian takes place by the radiation in the outside cores carrying out the Hamiltonian difference. Oscillations indicate the residual differences. For reference, red spatio-temporal iso-surfaces correspond to the central core, blue ones to the first circle of neighbouring cores (with peak power values 50 times less than in the central core).

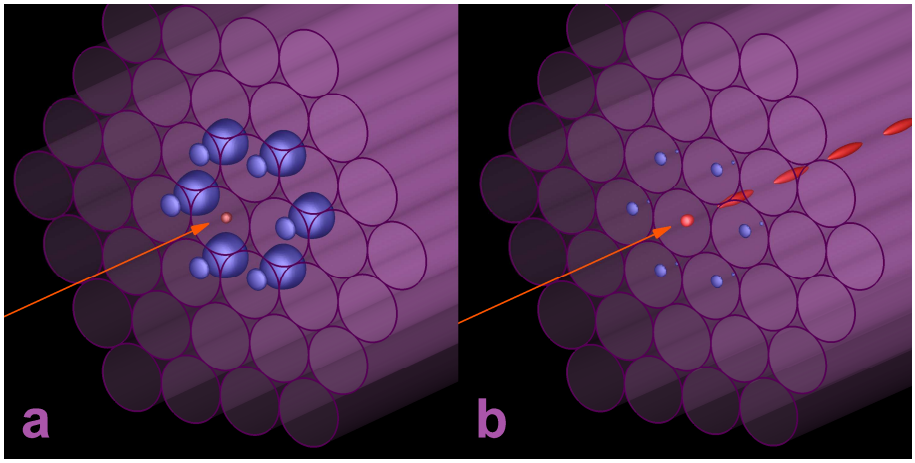

Figure 5 Power iso-surfaces of weak linear (a) and powerful nonlinear (b) input Gaussian pulses with the same energy during propagating along the hexagonal waveguide geometry

3. Nonlinear light bullets combining and compression in multicore fibers

The technology of optical multi-core fibers (MCFs) is one of the possible methods of implementing spatial-division multiplexing (SDM) for future high-capacity optical communications. A brute-force solution of the ever growing capacity problem is to deploy multiple communication systems over parallel fibers, in order to meet demand. However, the use of multiple systems over parallel fibres will lead to linearly scaled (with growing capacity) transmission costs and power consumption. The SDM technology might potentially enable a substantial reduction in cost-per-bit and improved energy efficiency. At the moment, however, SDM technology is in the research stage and major research activities worldwide are exploring and testing various MCF designs and this potentially disruptive new platform. In MCFs the optical pathways are defined by an array of physically-distinct single-mode cores. In conventional optical communications, the nonlinear effects that occur during signal propagation in a fiber due to the proximity of other data transmission channels are typically undesirable. An obvious approach to limiting cross-talk between spatial channels is to

keep the fiber cores well-spaced. Laboratory experiments demonstrate the feasibility of MCF technology for Pb/s fiber transmission.

The MCFs can also be used for very different, high power applications. At high signal power and coupling among cores, existing MCFs can be also considered as nonlinear discrete physical systems, interesting both for fundamental science and for various potential practical applications as nonlinear photonic devices. With a large number of cores, the continuous limit of discrete models in the form of the well-known nonlinear Schrödinger (NLS) equations can be used for a qualitative understanding of the system evolution. In particular, for propagation in MCFs with the so-called anomalous dispersion, the 2- and 3-dimensional NLS equations describe the well known effects of self-focusing and wave collapse. Specifically, pulse compression and concentration of the energy in a few fibers can be achieved.

When the energy is concentrated in a single core, the problem becomes effectively one-dimensional and the collapse stops. Hence the discreteness must limit the the combining and compression. The idea to use the collapse for pulse compression in fiber arrays was proposed more then 20 years ago, but to build the fiber arrays is an technological challenge. MCF is an example of a fiber array with a specific distribution of relatively low total number of cores in which the proposed ideas can be implemented. This type of nonlinear combining is substantially different from currently popular schemes of linear beam combining and can be advantageous for some other energy transfer and delivery applications.

In this report we focus on a theoretical study of the key underlying models and their mathematical properties. We consider two types of MCFs. In the first, the cores are placed as a ring in the fiber cross section with each core interacting with two neighbors only (see Fig. 3.1). In this case, the continuous model is the 2D nonlinear Schrödinger equation.

As a second example, we examine hexagonal or square positioning of the cores (2D core distribution, as shown in Fig. 3.2) with each core interacting with several (more than two, compared to the first case) neighbors, resulting in a stronger nonlinear interaction. The continuous model in this situation is the 3D NLSE. The evolution of NLSE collapsing solutions, both in 2D and in 3D, has been studied in detail. Using these classical results, we can obtain insight into the optimization of the energy localisation process.

In this project we have evaluated through numerical modelling optimal conditions for nonlinear pulse combining and compression in multi-core fibers. We demonstrated that the conditions for optimal combining and compression are substantially different. In the 7-core ring MCF we demonstrate a combining of 83.5% of energy into a single core and pulse compression over 300 times. In the 19-core ring MCF we find regimes with 80% energy combining and 720 times compression. Numerical modelling established that a 7-core hexagonal MCF allowed us to combine 91.6% of energy and to compress an optical pulse up to 256 times. In the case of a 19-core hexagonal fiber, we find regimes providing 80.9% energy combining and compression with a factor of 250. We demonstrate that the 2D distribution of the cores across the MCFs (see Fig. 3.2) increases the nonlinear interaction between the channels, but this does not result in improvement of the compression and combining efficiency compared to ring configurations. However, 2D placement of the cores greatly reduces the combining and compression length which can be useful and is an important feature for practical device design. Moreover, the combining and compression in a 2D MCF is more robust and insensitive to variation of the initial parameters. The analysis of the NLSE continuous limit helps us to understand these results.

Finally, we summarize the results of the optimisation for the combining and compression, and we present the optimal (within the considered schemes) MCF design. We also briefly discuss the possible practical devices and their parameters.

3A. Self-focusing and collapse in 2D and 3D

Let us re-write basic models discussed above in the dimension units now. The electromagnetic field of optical pulses propagating along MCF with 1D core distribution can be well approximated by a superposition of modes

$$E(x,y,z,t) = \\ = \sum_k A_k(z,t)F_k(x-x_k,y-y_k)e^{i(\beta_k z-\omega t)} + cc, \tag{3.1}$$

where F gives the spatial mode structure and A_k is the complex envelope of the electromagnetic field in core number k. In the limit of a weak-coupling approximation one can derive a system of equations for the envelopes A_k, i.e., the continuous-discrete nonlinear Schrödinger equation:

$$i\frac{\partial A_k}{\partial z} = \frac{\beta_2^k}{2}\frac{\partial^2 A_k}{\partial t^2} - \gamma_k|A_k|^2A_k - \sum_{m=1}^{N} C_{km}A_m, \tag{3.2}$$

where $k = 1,\dots,N$, β_2^k is the group-velocity dispersion parameter for the mode k, γ_k is the Kerr parameter, and the quantities C_{km} are the coupling coefficients between the cores. Consider first, the ring cores geometry (Fig. 3.1). Taking into account the interaction between nearest neighbors only, we can simplify the analysis with the following assumption

$$C_{k,k+1} = C > 0 \tag{3.3}$$

and neglect all other coupling terms. We consider $\beta_2^k = \beta_2 < 0$, $\gamma_k = \gamma$ $(k = 1,\dots,N)$.

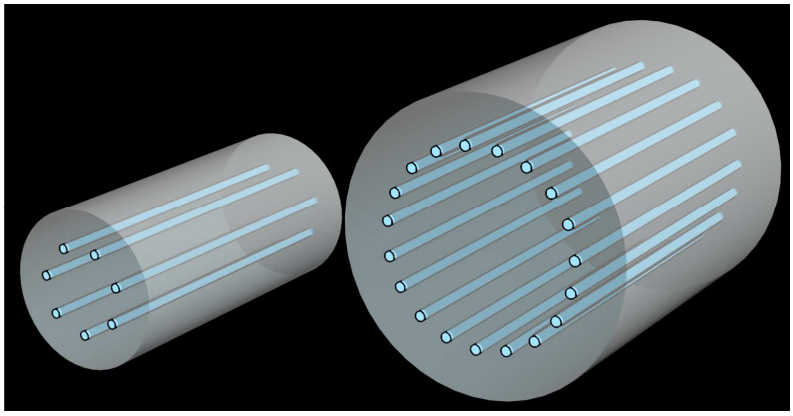

Figure 3.1 : Schematic depiction of the considered MCF waveguide with 7 (left) and 19 (right) cores arranged in a circle.

It is convenient to introduce normalized variables: $A_k = \exp(i2z')\sqrt{C/\gamma}U_k$, where $z' = z/L$, $L = 1/C$, $t' = t/T$, $T^2 = -\beta_2/(2C)$. The dimensionless equations (omitting the primes) read:

$$i\frac{\partial U_k}{\partial z} = -\frac{\partial^2 U_k}{\partial t^2} - (U_{k+1} - 2U_k + U_{k-1}) - |U_k|^2U_k. \tag{3.4}$$

In the case of a 2D core distribution we have the system for the envelopes $A_{n,m}$

$$i\frac{\partial A_{n,m}}{\partial z} = \frac{\beta_2}{2}\frac{\partial^2 A_{n,m}}{\partial t^2} - \sum_{k,l} C_{n,m,k,l}A_{kl} - \gamma|A_{n,m}|^2A_{n,m}. \tag{3.5}$$

Consider two different geometries, the square and hexagonal lattices (Fig. 3.2). We introduce normalized envelopes $A_{n,m} = \exp(i4z')\sqrt{C/\gamma}U_{n,m}$ for the square geometry and $A_{n,m} = \exp(i6z')\sqrt{C/\gamma}U_{n,m}$ for hexagonal geometry, where C is the same for all the neighboring cores coupling coefficient (other couplings may be neglected), and dimensionless variables $z' = z/L$, $L = 1/C$, and $t' = t/T$, $T^2 = -\beta_2/(2C)$, the same as for the ring geometry. Finally, omitting the primes, the system of NLSE takes the form:

$$i\frac{\partial U_{n,m}}{\partial z} + \frac{\partial^2 U_{n,m}}{\partial t^2} + (\underline{CU})_{n,m} + |U_{n,m}|^2 U_{n,m} = 0, \tag{3.6}$$

where $(\underline{CU})_{n,m}$ is the linear coupling profile at site (n,m). For the square and hexagonal core configurations, the combination $(\underline{CU})_{n,m}$ is given by expression

$$\begin{aligned}(\underline{CU})_{n,m}^{sqr.} &= U_{n-1,m} + U_{n+1,m} + U_{n,m-1} + U_{n,m+1} - 4U_{n,m} \\ (\underline{CU})_{n,m}^{hex.} &= U_{n-1,m-1} + U_{n+1,m-1} + U_{n-2,m} + \\ &\quad U_{n+2,m} + U_{n-1,m+1} + U_{n+1,m+1} - 6U_{n,m}.\end{aligned} \tag{3.7}$$

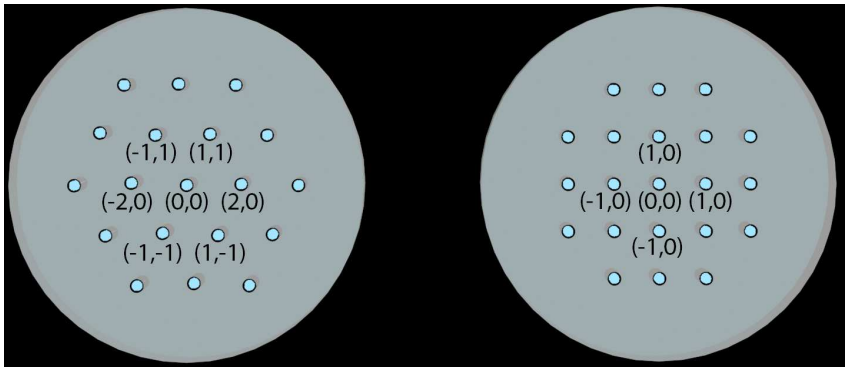

Figure 3.2: Schematic depiction of the considered multi-core fiber with hexagonal and square geometry and 2D numbering of cores.

The continuous-discrete NLSEs conserve the total energy (normalized by C/γ)

$$\begin{aligned}(1D): E &= \sum_{k=1}^{N}\int_{-\infty}^{\infty}|U_k(z,t)|^2 dt, \\ (2D): E &= \sum_{n,m}\int_{-\infty}^{\infty}|U_{n,m}(z,t)|^2 dt,\end{aligned} \tag{3.8}$$

and Hamiltonian

$$\begin{aligned}&(1D): \\ &H = \sum_{k=1}^{N}\int_{-\infty}^{\infty}\left[\left|\frac{\partial U_k}{\partial t}\right|^2 + |U_k - U_{k-1}|^2 - \frac{|U_k|^4}{2}\right]dt, \\ &(2D): \\ &H = \sum_{n,m}\int_{-\infty}^{\infty}\left[\left|\frac{\partial U_{n,m}}{\partial t}\right|^2 - (\underline{CU})_{n,m}U_{n,m}^* - \frac{|U_{n,m}|^4}{2}\right]dt\end{aligned} \tag{3.9}$$

and the master equations have the Hamiltonian structure:

$$i\frac{\partial U_{n,m}}{\partial z} = \frac{\delta H}{\delta U_{n,m}^*}. \tag{3.10}$$

The system (3.4) with a large number of cores and smooth intensity distribution that experiences only small changes between neighboring cores for the ring geometry (Fig. 1) is equivalent to the continuous 2D NLSE for $U(k,t,z)$:

$$i\frac{\partial U}{\partial z} + \frac{\partial^2 U}{\partial t^2} + \frac{\partial^2 U}{\partial k^2} + |U|^2 U = 0, \tag{3.11}$$

with Hamiltonian

$$H = \int_{-\infty}^{\infty}\left[\left|\frac{\partial U}{\partial t}\right|^2 + \left|\frac{\partial U}{\partial k}\right|^2 - \frac{|U|^4}{2}\right]dt. \tag{3.12}$$

Eq. (3.11) is equivalent to the NLSE that describes the self-focusing of light in various nonlinear media. The continuous analog can be used for insight in discrete system evolution.

In the conventional theory of self-focusing governed by the NLSE, the initial wave distribution collapses into singularity when the Hamiltonian H is negative, or when the beam power exceeds the critical value P_{cr}. This value depends on the beam shape and is minimal for the Townes mode. In our case, the role of power is played by the total energy injected into the MCF $E = \int dtdn|U_n|^2$. When the input energy exceeds the critical value E_0, (for the Townes beam, $E_0 = E_{cr} = 4\pi$, in terms of the dimensional variables $E_{cr} = 4\pi\sqrt{-C\beta_2/(2\gamma^2)}$), making $H < 0$, the intensity distribution is self-compressed over k and t. We can expect that the injected MCF pulses distributed over the cores with smooth maxima will be focused into a few cores around the maxima with simultaneous pulse compression. When the energy is concentrated into a few cores the discreteness of the cores arrests further compression. When the input energy $E >> 4\pi$, the distribution breaks into a few collapsing clusters with $E \approx 4\pi$ (similar to filamentation in the continuum limit). In every cluster the compression and combining takes place, but the location of the peaks is difficult to predict and this situation is not practical for the goals of beam combining or pulse compression.

The continuous version of the continuous-discrete 3D NSLE (Fig. 2) takes the form:

$$i\frac{\partial U}{\partial z} + \frac{\partial^2 U}{\partial t^2} + \frac{\partial^2 U}{\partial k^2} + \frac{\partial^2 U}{\partial l^2} + |U|^2 U = 0 \tag{3.13}$$

for $U(z,t,k,l)$, where the spatial variables k and l take the values of a certain bounded domain S (e.g. $S = \{(k,l): k^2 + l^2 < R^2\}$ for a circle of radius R). The Hamiltonian in this case has the following form:

$$H = \int_{-\infty}^{\infty}\int_S \left[\left|\frac{\partial U}{\partial t}\right|^2 + \left|\frac{\partial U}{\partial k}\right|^2 + \left|\frac{\partial U}{\partial l}\right|^2 - \frac{|U|^4}{2}\right] dkdldt. \tag{3.14}$$

An increase in the number of neighbours enhances the nonlinear interaction and makes collapse possible even for positive values of H. In this case we can expect that the injected MCF pulses will be focused into a few central cores with simultaneous pulse compression. Nonlinear systems described by equation (3.13) have stronger collapsing features, and a MCF with 2D configuration of cores could demonstrate better compression results, which will be shown later. In the 3D situation, the collapse is ``weak'' and the energy involved in the compression processes decreases. In this case, the optimal compression and combining is reached in a transient regime and the choice of parameters is not universal. We will present the results of the modeling of compression and combining in both situations and will examine the selection of the optimal parameters.

3B. 2D compression and energy combining in 7-core and 19-core ring MCFs

First we consider pulse evolution in MCFs with the ring design shown in Figure 3.1. The 7-core and 19-core MCFs with the cores arranged in a circle are considered. The analysis of pulse compression and combining in a MCF with 1D location of the cores was carried out for the initial conditions given by the same Gaussian pulses in each core:

$$U_k(0,t) = \sqrt{P}\exp\left(-\frac{t^2}{2\tau^2}\right)\left[1 + M\cos\left(\frac{2\pi k}{N}\right)\right], \tag{3.15}$$

where M is the modulation coefficient, and $k = 1,\ldots,N$. The modulation $M\cos(2\pi k/N)$ produces the smooth initial intensity modulation with a maximum in the designated core. This modulation accelerates the compression, and most importantly, makes it less sensitive to the perturbation of the initial parameters. On the other hand, the perturbation must be small enough for the efficient utilisation of each core ($M << 1$).Here we present the optimal parameters for the most efficient system performance for $M = 0.3$.

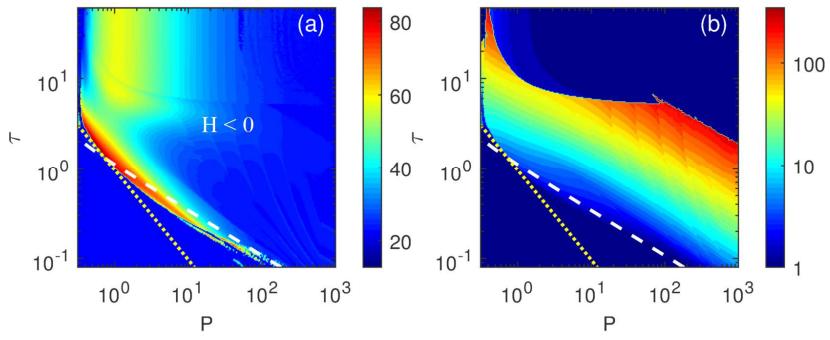

Figure 3. 3: Dependence of the percentage of total energy E combined in the core with pulse compression (a) and the pulse width compression factor (b) on the initial pulses [Eq. (3.15)] parameters P and τ for 7-core MCF with ring core configuration and modulation coefficient $M = 0.3$. The isoline $E = E_{cr} = 4\pi$ is indicated by the yellow dots, the level $H = 0$ is depicted by white dashes.

We perform simulation of light pulse propagation initially distributed according to Eq. (3.15) aiming at the optimisation of pulse compression and energy combining. The dependencies of the basic compression parameters are obtained for the range of parameters $P \in [0.31; 1000]$, $\tau \in [0.05; 60]$ for the 7-core MCF and $P \in [0.05; 1000]$, $\tau \in [0.05; 230]$ for the 19-core MCF. Numerical modelling was performed by the split-step Fourier method with the Padé approximation with scaling and squaring for the matrix exponential.

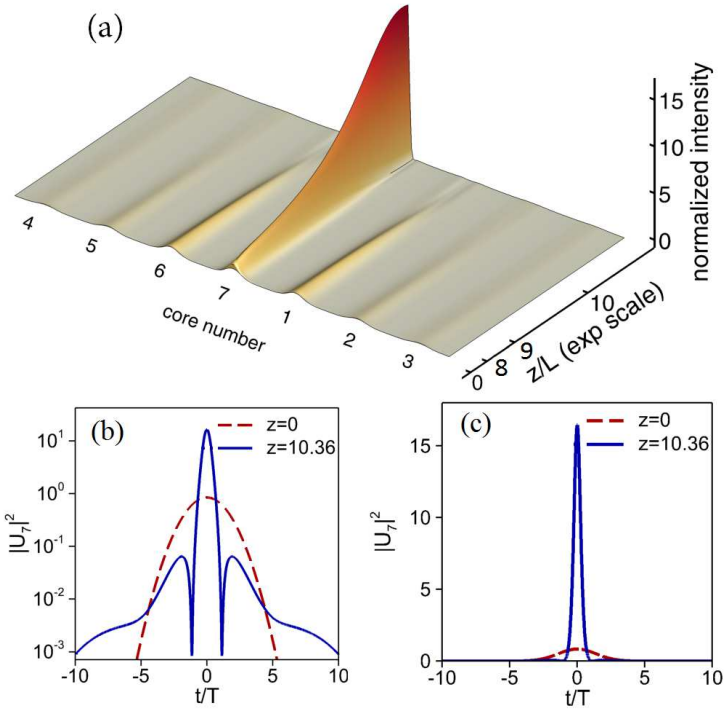

Figure 3.4: Evolution of the input Gaussian pulses [Eq. (3.15)] with the parameters $P = 0.5$ and $\tau = 2.0$ injected in all cores of ring 7-core MCF (a). Corresponding input intensity distribution in core 7 (red color) and the distribution at compression point (blue color) are shown in logarithmic (b) and normal (c) scales.

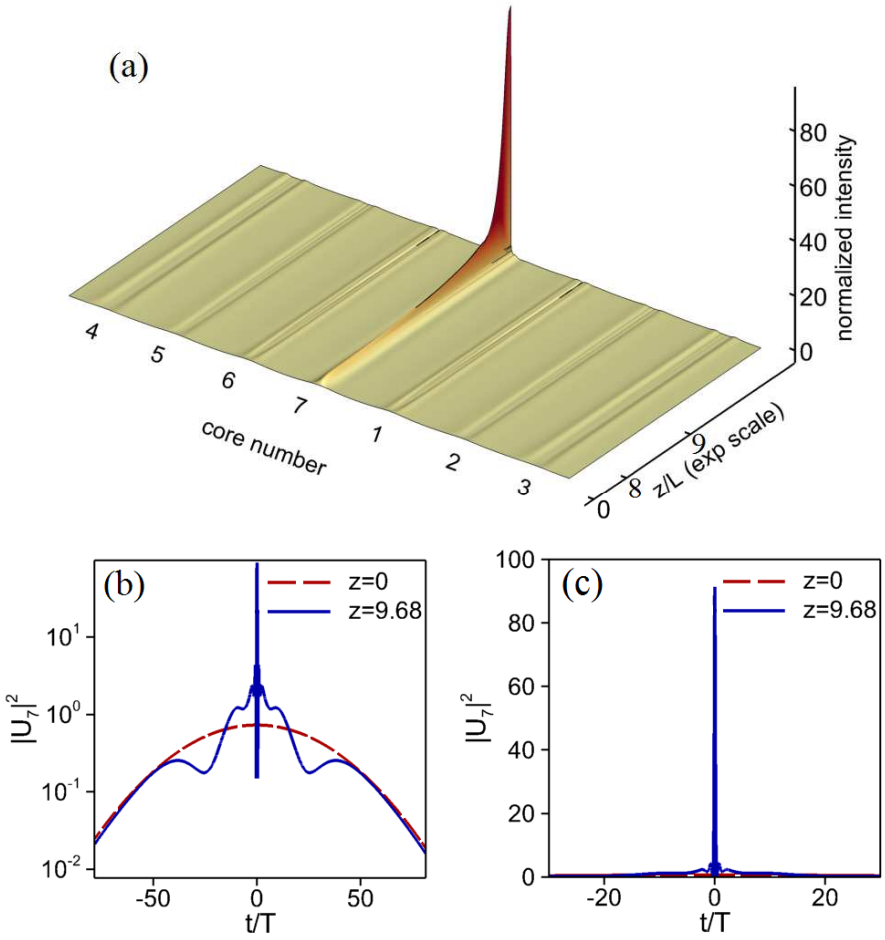

Figure 5: Evolution of the input Gaussian pulses [Eq. (3.15)] with the parameters $P = 0.436$ and $\tau = 42.5$ injected in all cores of ring 7-core MCF (a). Corresponding input intensity distribution in core 7 (red color) and the distribution at compression point (blue color) are shown in logarithmic (b) and normal (c) scales.

The range of values of the initial pulse parameters P and τ was discretized by 250×250 nodes. For each parameter pair (P, τ) of the grid, the simulation of the dynamics of optical pulses with the form (3.16) injected into every core of the appropriate MCF was made. We tracked the first peak power maximum of the propagating pulse to get the compression or energy conversion at the minimum possible distance along the fiber. In what follows we call such a distance an ``optimal" one. Moreover, we took into account only those maxima at which peak power is increased by more than $0.2N$ times, where N is the number of cores ($N > 5$). This approach was applied to cut-off the situations when the peak power maximum is observed without the pulse compression. The value $0.2N$ was chosen empirically. When the energy E is comparable with E_{cr}, the particular initial distribution is not optimal and it can have a few oscillations before the collapse (here - sharp energy localisation to few cores). In this situation, even when strong compression and combining takes place, the position of peaks is sensitive to the initial perturbation and, for the purpose of this study, we consider the situation as not practical. The above procedure eliminates this type of dynamics. It is worth noting that in the general case the parameters for the optimal temporal pulse compression and maximum energy combining in a single core are different, and the distances along the fiber z_0 of maximum compression and combining are also varying in modelling.

The maps of combining and compression performance for the 7-core ring MCF are presented in Fig. 3.3. In Fig. 3.3a we see the coherent effective beam combining. For the optimal

choice of parameters, 83.5% of the initial energy is combined in one core at the distance 10.36 (in the dimensionless variable z). The combined pulse is smooth, and the side satellite peaks have an intensity of 4% of the peak intensity. The total energy in the wings is about 1.9%. Note that the region of the maximal combining lies close to the line $H = 0$. The map of the compression efficiency is quite different. The blue area denotes pairs of parameters P and τ, for which there is no pulse compression or the initial pulses (3.15) break into clusters as a result of the modulation instability. It is interesting that isolines of pulse compression factor in Fig. 3b correlate with isolines of the ratio of the dispersion length $L_D = \tau^2/|\beta_2|$ and the nonlinear length $L_{NL} = 1/(\gamma P)$. The zone of optimal compression is the stripe narrowing toward high total energies and is confined by the level $L_D/L_{NL} \approx 3000$. If $L_D/L_{NL} > 3000$, a large nonlinearity destroys a smooth pulse shape before the compression point. In the area of P and τ values for which the compression occurs, the compression factor of up to 307 times can be obtained. The maximal compression is reached at the distance $z = 9.68$.

The evolution of the peak intensities in the different cores in the case of optimal combining (83.5% of all energy combines in the single core) is presented in Fig. 3.4. We see that the combined pulse has a smooth temporal shape with low-intensity wings. The length of combining is about 10.36 in dimensionless units, due to the slow initial development. In the final stage, as one can see in Fig. 3.4a, the intensity growth is about exponential. The pulse compression is modest (about 6 times).

The evolution of the intensity in the different cores for the case of maximal pulse compression is presented in Fig.3. 5. The pulse compressed over 300 times. The compressed pulse is still mainly smooth, with noticeable wings. In this case, only about 36% of the energy combined in the compressed pulse. The interesting feature of the compression is a long initial evolution which is consistent with high sensitivity to the initial conditions.

To obtain insight for the optimal parameters for the compression and combining, let us use the continuous limit. For classical self-focusing the collapse takes place at $P > P_{cr}$. At powers well above P_{cr}, the beam breaks into filaments with a power close P_{cr}. Using the similarity of our problem with self-focusing, we can expect that for the optimal operation the total energy $E > E_{cr}$. For $E >> E_{cr}$ we must have the undesirable filamentation, energy concentration in a few different cores, and temporal modulations of the pulses. The results of the combining modeling are consistent with the above arguments. The parameter area where pulse compression occurs is easily distinguishable and is confined near the line $H = 0$. For optimal combining, the size of the distribution over cores and the temporal width must be comparable. As a result, we can expect that the optimal pulse duration for the combining must increase proportionally to N. The optimal combining corresponds to almost complete concentration in one core. The pulse compressed about 6 times, which indicates the collapse of the distribution as a whole.

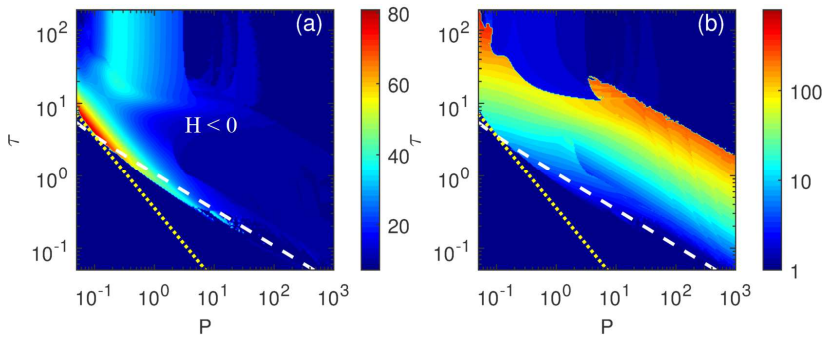

Figure 3.6: Evolution of the input Gaussian pulses [Eq. (3.15)] with the parameters $P = 0.09$ and $\tau = 4.33$ injected in all cores of the ring 19-core MCF (a). The input intensity distribution in core 19 (red color) and the distribution at compression point (blue color) are shown in logarithmic (b) and normal (c) scales.

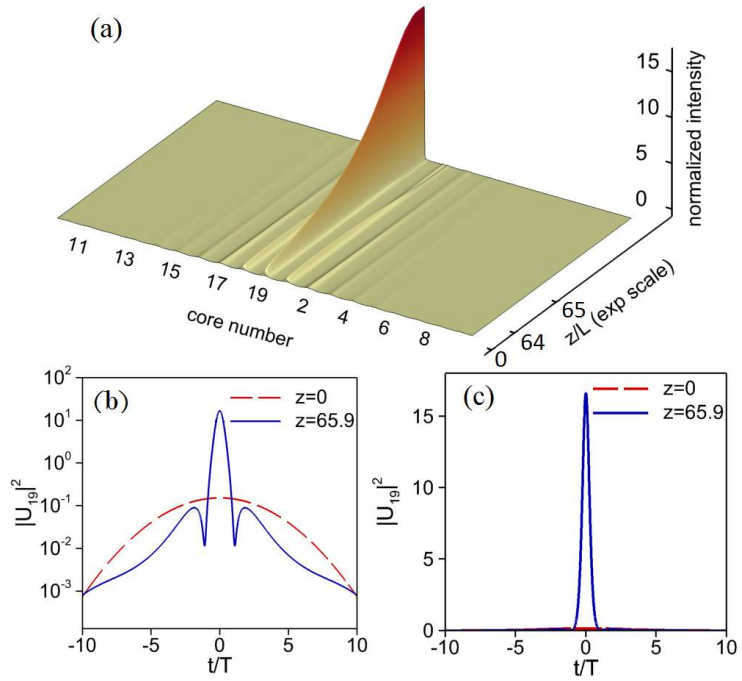

Figure 3.7: Evolution of the input Gaussian pulses [Eq. (3.15)] with the parameters $P = 0.0545$ and $\tau = 184.0$ injected in all cores of the ring 19-core MCF (a). The input intensity distribution in core 19 (red color) and the distribution at compression point (blue color) are shown in logarithmic (b) and normal (c) scales.

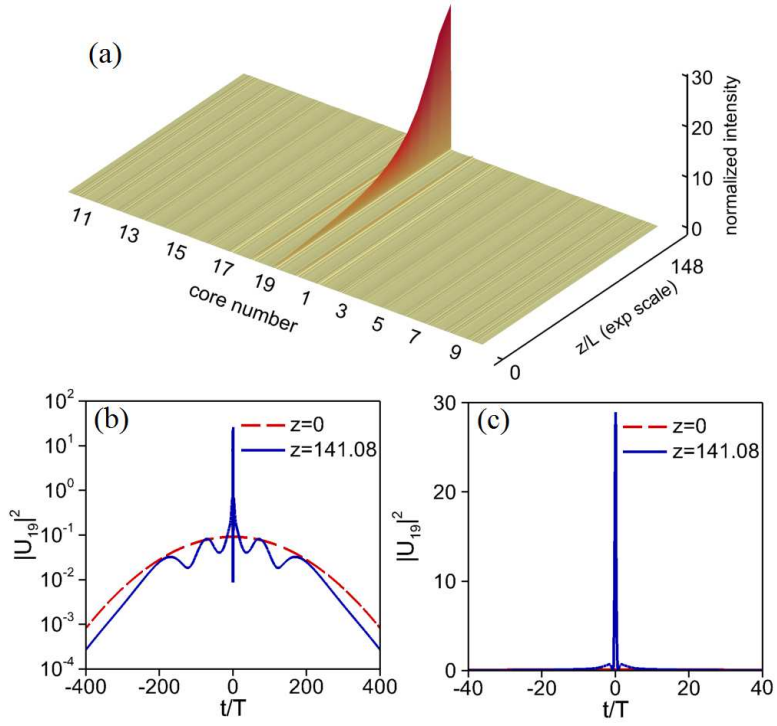

Figure 3.8: Dependence of the percent of total energy E combined in the core with pulse compression (a) and the pulse width compression factor (b) on the initial pulses [Eq. (3.15)] parameters P and τ for the 19-core MCF with ring core configuration and modulation coefficient $M = 0.3$. The isoline $E = E_{cr} = 4\pi$ is indicated by the yellow dots; the level $H = 0$ is depicted by white dashes.

The maps of the efficiency of the combining and compression for the 19-core ring MCF are presented in Fig. 3.8. Qualitatively, the maps are similar to the case of 7 cores with higher sensitivity to the initial condition. The maximal efficiency of combining is about the same as for 7 cores and qualitatively the behavior is similar (see Fig. 6), but the compression distance z is much larger, namely 65.9. For the maximum combining, the compression of the pulse is higher according the above discussion.

The maximal compression was obtained by the initial pulses with $L_D/L_{NL} \approx 3000$ and approximately equals 720, and the compressed pulse has a smooth profile (see Fig. 3.7). With increase of the number of cores the optimal conditions for the maximal compression become more sensitive to the initial conditions. Also, the distance to the compression point increases and is equal to 141.08.

3C. Compression and combining in hexagonal and square MCF

In this section we consider the optical MCFs with 2D core distribution design -- in nodes of square and hexagonal grid shown in Figure 2. Let us start with a discussion of the continuous limit, considering the evolution of the intensity distribution according [eq. (3.13)]. The collapse of the distribution in 3D (cores, coordinates, and time) takes place even for positive values of the Hamiltonian. It is clear that the boundary value of $H = H_c$ corresponds to the z-independent (``stationary") localized solution. The distributions with $H < H_c$ collapsed. The collapse within the 3D NLSE is weak, and the energy leaks from the collapse. This means that it is not beneficial to greatly increase the number of cores, and efficient combining and compression take place in the transient regime, sensitive to the boundary conditions. As was already mentioned above, the initial distribution is not optimal for the collapse. The optimum for the beam combining is different from the optimum for beam compression (analogue of 3D collapse).

A comprehensive analysis of pulse compression and combining in MCF with 2D location of the cores was carried out for initial pulses having the same Gaussian profile in each core, namely

$$U_{n,m}(z=0,t) = \sqrt{P}\exp\left(-\frac{t^2}{2\tau^2}\right), \tag{3.16}$$

We compare the efficiency of a 7-core and 19-core MCF with hexagonal core distribution and 21-core MCF with square core configuration. The dependencies of basic compression parameters are shown for the same range of parameters P, τ as in the case of the ring MCFs.

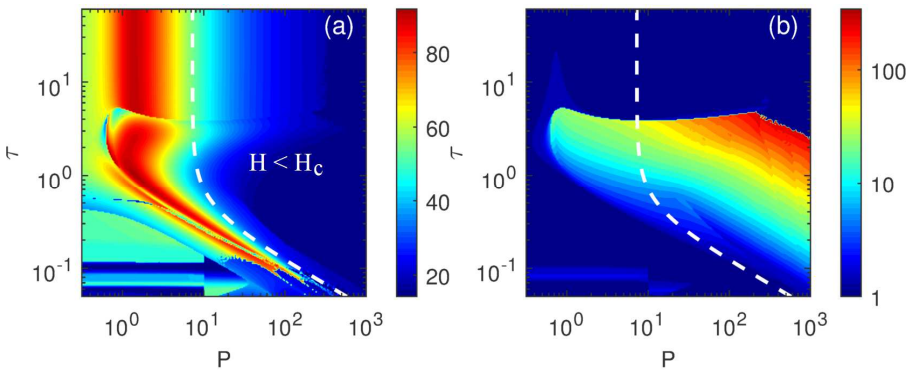

Figure 3.9: Dependence of the percent of total energy E combined in the core with pulse compression (a) and the pulse width compression factor (b) on the initial pulses [Eq. (3.15)] parameters P and τ for 7-core hexagonal MCF without modulation. The level $H = H_c$ is depicted by white dashes.

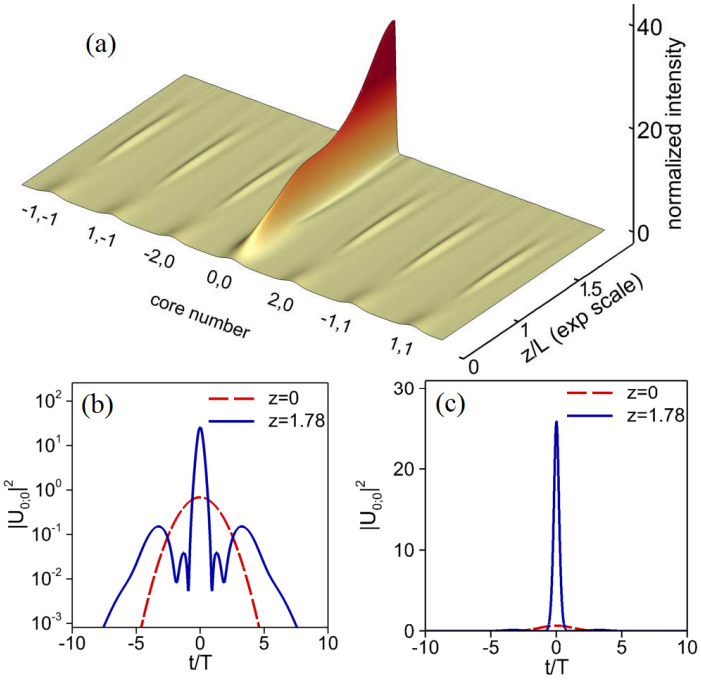

Figure 3.10: Evolution of the input Gaussian pulses [Eq. (3.15)] with the parameters $P = 0.687$ and $\tau = 1.775$ injected in all cores of hexagonal 7-core MCF (a). The input intensity distribution in the central core (red color) and the distribution at compression point (blue color) are shown in logarithmic (b) and normal (c) scales.

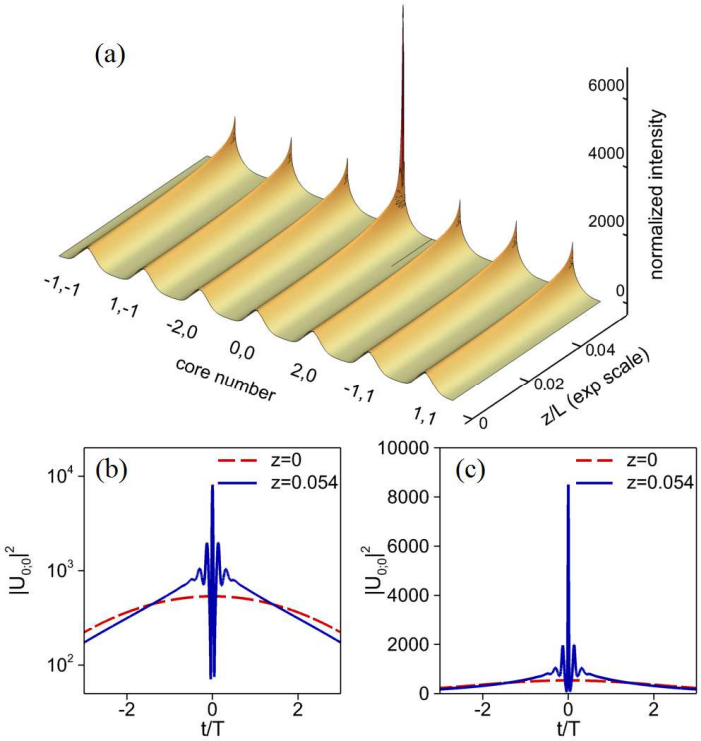

Figure 3.11: Evolution of the input Gaussian pulses [Eq. (3.)] with the parameters $P = 536$ and $\tau = 3.2$ injected in all cores of hexagonal 7-core MCF (a). The input intensity distribution in the central core (red color) and the distribution at compression point (blue color) are shown in logarithmic (b) and normal (c) scales.

First, we consider the hexagonal MCFs. The maps of the pulse combining and compression for 7 cores case are presented in Fig. 3.9. The blue area denotes pairs of parameters P and τ, for which there is no pulse compression, or the initial pulses (3.15) with this parameters break into filaments or are compressed after the distance along the fiber where the first local maximum of peak power is located. Due to the symmetry of the problem, both combining and compression take place in the (0,0) core. We see that the optimal conditions for combining and compression are very different from the the results for the ring cores distribution (Fig. 3.3). The optimal parameters for the compression are very different from combining similar to the ring MCF. Efficient combining takes place in a much broader range of parameters in the vertical band, insensitive to the pulse duration. This indicates that collapse takes place mainly in the transversal direction. The efficiency of combining and compression is comparable with the ring MCF, but much less sensitive to variation of the initial parameters. The maximum combining efficiency for a 7-core hexagonal MCF is better and equals 91.6% (Fig. 3.10) at the distance $z = 1.78$. In contrast to the ring core configurations, a wide region in the plane of parameters (P, τ) exists, where the part of the energy in the central core at the compression moment exceeds 70% of the initial energy E. The presence of this region allows us to obtain well-compressed pulses having most of the total energy E, which is of great practical importance. However, in this case a substantial part of the energy goes into the wings, rather than into the central peak of the compressed pulse.

An increase in the number of cores to 19 (Fig. 3.14) does not qualitatively change the map, and the maximal efficiency of combining is about 80.9%. Optimal combining takes place in a vertical band of parameters. The independence of the combining efficiency form the pulse duration indicates a 2D collapse in m,n variables. Another indication of the 2D nature of the combining process is that the band of the high combining efficiency is limited by the line $H = 0$, which for long pulses coincides with the 2D collapse criteria. The distance along the 19-core hexagonal fiber to the point at which the best combining occurs equals $z = 2.07$.

The distribution over cores can collapse even without pulse compression. In Figs. 3.9 and 3.12 one can see that it is possible to obtain efficient combining practically without compression. In a 2D MCF, combining and compression typically go together with different rates.

Using the 7-core fiber, a maximal pulse compression up to 256 times can be achieved (Fig. 3.11). In contrast to the combining pattern, at the point of maximal compression a significant fraction of energy is left in the neighbor cores. The peak power increases greatly at the compression point. The best compression occurs in the case of a high power input pulse. Too much nonlinearity ($L_D/L_{NL} \approx 4000$) destroys the pulse shape before the compression point and confines the maximal pulse compression factor. On the other hand, it is difficult to define the optimal compression case in the presence of high nonlinearity. The pulse compression factor close to its maximal value can be obtained for different pairs of parameters P, τ and the distance to these compression points decreases with growth of the parameter P. The compression distance is sufficiently small for both the 7-core and the 19-core hexagonal MCFs ($z \leq 0.1$ and $z \leq 0.5$, respectively).

The pulse shapes after compression and combining and the intensity evolutions are presented in Fig. 3.10—3.13. As in the ring cores geometry, the compressed pulse has a smooth shape and the energy is localized mainly in one central core.

As we discussed, one can expect that the efficiency of combining and compression can degrade with increasing number of cores, but the total energy in the central cores continue to grow. The stronger nonlinear interaction for a 2D MCF does not increase the efficiency of compression (combining) but greatly reduces the required distance and increases the process robustness.

Summing up, the 7-core hexagonal MCF offers a better combining than the 19-core ring MCF, but the latter one can provide higher level of compression.

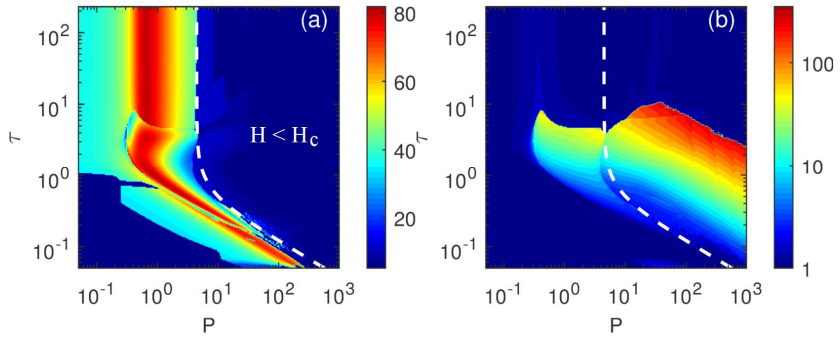

Figure 3.12: Dependence of the percent of total energy E combined in the core with pulse compression (a) and the pulse width compression factor (b) on the initial pulses [Eq. (3.15)] parameters P and τ for the 19-core hexagonal MCF without modulation. The level $H = H_c$ is depicted by white dashes.

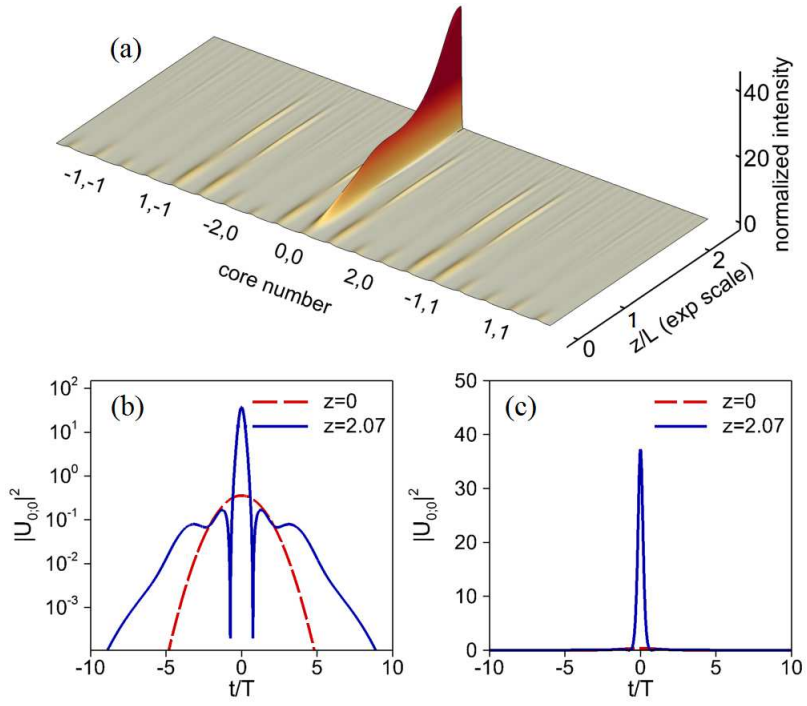

Figure 3.13: Evolution of the input Gaussian pulses [Eq. (3.15)] with the parameters $P = 0.36$ and $\tau = 1.69$ injected in all cores of a hexagonal 19-core MCF (a). The input intensity distribution in the central core (red color) and the distribution at compression point (blue color) are shown in logarithmic (b) and normal (c) scale.

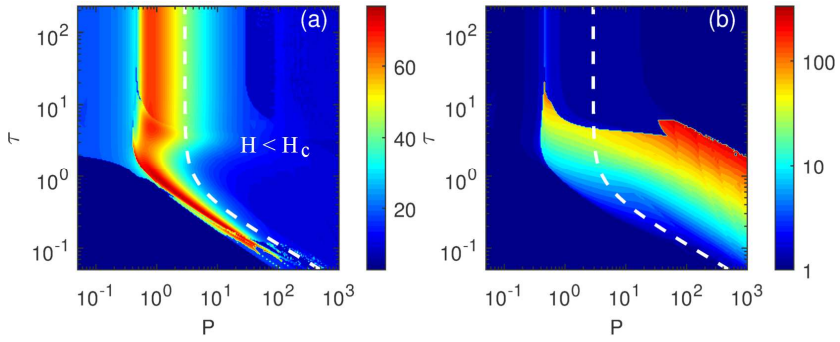

Figure 3.14: Dependence of the percent of total energy E combined in the core with pulse compression (a) and the pulse width compression factor (b) on the initial pulses [Eq. (3.15)] parameters P and τ for hexagonal 19-core MCF with modulation coefficient $M = 0.3$. The level $H = H_c$ is depicted by white dashes.

Furthermore, we have tried to improve the combining scheme using a 19-core hexagonal MCF, and we have also studied its stability against modulation. First, the effect of amplitude modulation of initial pulses on compression characteristics was considered (see Fig. 3.14). Initial conditions were given by the same Gaussian pulses in each core, but the amplitudes from core to core was slightly perturbed, depending on the distance to the central core:

$$\tilde{U}_{n,m}(0,t) = \\ = \sqrt{P}\exp\left(-\frac{t^2}{2\tau^2}\right)\left[1 + M\cos\left(\pi\frac{n^2+3m^2}{N^2}\right)\right], \quad (3.17)$$

Here N is the maximum modulus index of a core (n or m) and M is the modulation coefficient. For calculations the value $M = 0.3$ was chosen, as in the case of ring core configurations. The influence of modulation is not as dramatic as in the case of ring MCFs, but it still has the same features. The compression region in the plane of the parameters (P, τ) is widened due to the increased robustness of the compression scheme. The absolute width of compressed pulses and pulse compression factor are less by $5 - 10\%$ as compared with a case $M = 0$, as caused by lower level of the total energy. Also the peak power increase factor lessened by up 2 times. The distance to the point of compression is less by up to 20%. The portion of the total energy E combined at the central core and at the central peak of the pulse have approximately the same order (Fig. 3.14b).

Let us now discuss the 2D core configuration with a square lattice and 21 cores. Our calculations showed that there is no noticeable difference between the square MCF and the 19-core hexagonal MCF, so we do not present figures for this type of MCF. The pulse compression factor for the hexagonal MCF is slightly smaller compared to the square MCF, and the peak power increase factor is larger for the square MCF, but these two facts can be explained by the increased number of cores ($N = 21$) and larger value of the total energy E. On the other hand, the maximum number of neighboring cores for the square MCF is less than for the hexagonal MCF (4 rather than 6), so the distance to the compression point is larger for the square MCF.

Table: Pulse parameters for maximum combining and maximum compression regimes for various types of MCFs.

MCF type and number of cores	Maximum combining [%]	Distance to the maximum combining point	Energy of combined pulse	Reduction of combined pulse's duration (FWHM)	Maximum compression (FWHM)	Distance to the maximum compression point	Duration of compressed pulse
Ring 7	83.5	10.36	12.97	5.74	307.6	9.68	0.23
Ring 13	75.4	14.79	14.78	16.1	569.0	47.32	0.42
Ring 19	80.0	65.90	13.71	12.7	720.4	141.08	0.39
Square 9	91.3	3.27	12.78	6.25	≈ 250	< 0.4	$\approx 0.02 - 0.07$
Square 13	82.1	2.85	14.42	6.01	≈ 250	< 0.6	$\approx 0.02 - 0.06$
Square 21	80.7	3.57	16.03	5.74	≈ 250	< 1.1	$\approx 0.02 - 0.09$
Hex 7	91.6	1.78	15.13	6.37	≈ 260	< 0.1	≈ 0.02
Hex 13	84.7	0.99	24.44	5.00	≈ 250	< 0.2	$\approx 0.02 - 0.03$
Hex 19	80.9	2.07	20.49	7.30	≈ 250	< 0.6	$\approx 0.02 - 0.07$
Hex 31	75.0	1.37	43.47	5.28	≈ 240	< 0.9	$\approx 0.02 - 0.07$
Hex 37	70.7	1.47	58.67	4.87	≈ 250	< 1.3	$\approx 0.02 - 0.08$

CONCLUSIONS

In this report we presented results of study on a spatio-temporal continuous-discrete model of an optical medium consisting of a multi-core fiber or a general array of waveguides which as this and other recent work indicates, can be used in a variety of applications. We have put forward a solid theoretical framework based on asymptotics and stability conditions that not only validates the existence of stable light bullets, representing light localization in space and time, but it shows these are not only achieved for a particular array configuration and instead are generic and stable for a multitude of geometries. This can represent an opportunity to design array configurations whose topology is suitable for a particular application including preparing a LB for propagation in bulk Kerr-media [19]. It can also be a starting point in the study other phenomena in nonlinear arrays when the model can be easily extended by incorporating additional effects. Two relevant examples that come to mind, are first the inclusion of higher order temporal effects which can be important for the most intense (and temporarily short) bullets. There is an additional time shift that is λ dependent (for λ large), then one should be able to verify it theoretically. Clearly such dependence would be quite useful for time delay lines and for efficient coherent pulse combining [20]. The second extension that comes to mind is coupling active fibers, where at first approximation we can add to the model linear gain and saturation. Finally we limited our work to the study of light bullets in the anomalous regime. A natural extension is to perform similar studies to discrete spatio-temporal vortices and other nonlinear modes. With respect to the normal regime, recent experimental results [21] demonstrate the existence of X-waves in 1d-semiconductor waveguide arrays. Theoretically, X-waves carry infinite energy, so once a proper renormalization of Power and the Hamiltonian is done to the work presented here, an improved existence and stability analysis to 1d and 2d arrays n the normal dispersion regime could be done. The obtained theoretical results have been verified using numerical simulations.

We have demonstrated that a MCF fiber can be effectively used for coherent wave combining and compression. The degree of compression can be continuously changed by varying

the incident beam parameters. We have demonstrated the possibility of compression exceeding a few hundred and coherent combining with efficiency over 80%. For a smooth distribution of energy, the evolution of the intensities in the cores is described by NLSE -- 2D for the ring cores distribution and 3D for the hexagonal and square cores structures. The well-studied collapse phenomena provide insight in the processes of beam combining and compression. We have demonstrated that the combining process is consistent with collapse phenomena. However, the maximal compression regime is qualitatively different from, and the maximal compression greatly exceeds, what one can expect from the collapse model.

We have demonstrated that for the ring MCF the efficiency of compression and combining can grow with an increase in the number of cores, but the results becomes increasingly sensitive to the initial conditions. Also the length of interactions increases with the number of cores.

For a hexagonal MCF, the efficiency of combining and compressing generally degrades with increasing number of cores, but the process is more robust and insensitive to the initial conditions. Also the interaction length is greatly reduced. This potentially makes the hexagonal MCF the best option among the considered ones for practical applications.

The above results were presented in terms of dimensionless variables, so as to be generic. Let us discuss the results in dimensional variables, choosing some specific possible applications. The typical length of interaction is a $1/C$, where C is the coupling coefficient. For a typical telecom C values for MCF $C = 15.7$ 1/km and the typical length is about 64 m. The time scale $T = \sqrt{-\beta_2/(2C)}$ is about 0.8 ps. The typical scale of energy $E = CT/\gamma = 10$ pJ.

A practical device can be based on the piece of MCF. It is technically difficult to make MCF with uniform coupling over the entire length (the effect of coupling spatial dependence will be discussed in the separate paper). To make a practical device, it is desirable to reduce the length of interaction. This means that one has to increase the coupling coefficient. The reduction of length to about one meter makes it easier to keep C uniform along the MCF. In this case, the typical scale of time is 100 fs and the typical energy is about nJ. We demonstrated that it is possible to combine pulses with energy $: 1000 E_{cr} \approx 1$ μJ. By changing the parameters, it is possible to compress pulses from ps to tens of fs.

For the hexagonal MCF, it will be possible to effectively combine energy for a wider range of pulse durations. For the above parameters we can combine pulses with durations of a hundred femtoseconds to a few picoseconds.

The compressions using the hexagonal MCF can shorten the pulse down to a femtosecond duration, with an intensity increase up to 270 times. For such a short pulse, of course, the Kerr model of nonlinearities ceases to apply and must be generalized to a temporally nonlocal one; the limits of compression would then require special studies.

Management

The payment on the project was delayed by more than nine months due to unknown reason, therefore, some change of the original plan was required. However, risk mitigation actions have been done and the project delivered all the research objectives.

REFERENCES

[1] A. B. Aceves, C. DeAngelis, A. M. Rubenchik and S. K. Turitsyn, "Multidimensional Solitons in Fiber Arrays", Opt. Lett. **19**, 329-331 (1994).

[2] A. B. Aceves, G. G Luther, C. DeAngelis, A. M. Rubenchik and S. K. Turitsyn, "Energy Localization in nonlinear fiber arrays: Collapse effect compressor", Phy. Rev. Lett. **75**, 73-76 (1995).

[3] F. Y. M. Chan, A. P. T. Lau, and H.-Ya. Tam, "Mode coupling dynamics and communication strategies for multi-core fiber systems", PRL 112, 193901 (2014) Opt. Express **20**, 4548 (2012).

[4] B. Zhu, T. F. Taunay, M. F. Yan, J. M. Fini, M. Fishteyn, E. M. Monberg, and F. V. Dimarcello, “Seven-core multicore fiber transmissions for passive optical network”, Opt. Express **18**, 11117 (2010)

[5] S. Minardi, F. Eilengerber, Y. K. Kartashov, A. Szameit, U. Ropke, J. Kobele, K. Schuster, H. Bartelt, S. Nolte, L. Torner, F. Lederer, A. Tunnermann and T. Pertsch, “Three-dimensional light bullets in arrays of waveguides”, Phys. Rev. Lett **105**, 293901 (2010); F. W. Wise, “Generation of light bullets”, Physics **3**, 107 (2010).

[6] F. Eilenberger, S. Minardi, A. Szameit, U. Ropke, J. Kobelke, K. Schuster, H. Bartelt, S. Nolte, L. Torner, F. Lederer, A. Tunnermann, and Th. Pertsch, “Evolution dynamics of discrete-continuous light bullets”, Phys. Rev. A **84**, 013836 (2011)

[7] B. M. Shalaby, V. Kermene, D. Pagnoux, A. Desfarges-Berthelemot, Barthelemy, A. Popp, M. Abdou Ahmed, A. Voss and T. Graf, "19-cores Yb-fiber laser with mode selection for improved beam brightness," Applied Physics B: Lasers and Optics **100**(4), 859-864 (2010)

[8] H-J. Otto, A. Klenke, C. Jauregui, F. Stutzki, J. Limpert and A. Tünnermann, “Scaling the mode instability threshold with multicore fibers”, to appear Optics Letters (2014).

[9] Y. Silberberg, "Collapse of optical pulses," Optics Letters. **15**, 1282 (1990).

[10] A. B. Blagoeva, S. G. Dinev, A. A. Dreischuh and A. Naidenov, "Light bullets formation in a bulk media," IEEE Journal of Quantum Electronics. **QE-27**, 2060 (1991).

[11] D. E. Edmundson and R. H. Enns, "Bistable light bullets," Optics Letters. **17**, 586 (1992); "The particle-like nature of colliding light bullets," Physical Review A. **51**, 2491 (1995).

[12] F. Wise and P. Trapani, “The hunt for light bullets - spatiotemporal solitons,” Opt. Photonics News **13**, 28-
32 (2002).

[13] B. A. Malomed, D. Mihalache, F. Wise, and L. Torner, “Spatiotemporal optical solitons,” J. Opt. B **7**, R53–
R72 (2005); .L. Torner, S. Carrasco, J. P. Torres, L. C. Crasovan, and D. Mihalache, “Tandem light bullets,” Opt. Commun. **199**, 277-281 (2001).

[14] A. S. Sukhorukov and Y. S. Kivshar, “Slow-Light Optical Bullets in Arrays of Nonlinear Bragg-Grating
Waveguides,” Phys. Rev. Lett. **97**, 233901 (2006).

[15] F. Eilenberger, S. Minardi, A. Szameit, U. Röpke, J. Kobelke, K. Schuster, H. Bartelt, S. Nolte, A. Tünnermann, and Th. Pertsch, "Light bullets in waveguide arrays: spacetime-coupling, spectral symmetry breaking and superluminal decay [Invited]," Opt. Express **19**, 23171-23187 (2011)

[16] E. W. Laedke, K. H. Spatschek, and S. K. Turitsyn, “Stability of discrete solitons and quasicollapse to
intrinsically localized modes,” Phys. Rev. Lett. **73**, 1055-1058 (1994).

[17] E. W. Laedke, K. H. Spatschek, S. K. Turitsyn and V. K. Mezentsev, “Analytic criterion for soliton instability in a nonlinear fiber array”, Phys. Rev. E **52**, 5549-5554 (1995).

[18] V. K. Mezentsev, S. L. Musher, I. V. Ryzhenkova and S. K. Turitsyn, JETP Lett. **60**, 829-835 (1994).

[19] D. Majus, G. Tamošauskas, I. Gražulevičiūtė, N. Garejev, A. Lotti, A. Couairon, D. Faccio, and A. Dubietis, "Nature of Spatiotemporal Light Bullets in Bulk Kerr Media", Phys. Rev. Lett. **112**, 193901 (2014).

[20] Marco Kienel, Michael Müller, Stefan Demmler, Jan Rothhardt, Arno Klenke, Tino Eidam, Jens Limpert, and Andreas Tünnermann, "Coherent beam combination of Yb:YAG single-crystal rod amplifiers", Opt. Lett. **39**, 11 (2014).

[21]Yoav Lahini, Eugene Frumker, Yaron Silberberg, Sotiris Droulias, Kyriakos Hizanidis, Roberto Morandotti and Demetrios N. Christoulides, "Discrete *X*-Wave Formation in Nonlinear Waveguide Arrays", Phys. Rev. Lett. **98,** 023901 (2007)